Three-dimensional imaging of a Ag-Au-rich epithermal system in British Columbia, Canada, using airborne z-axis tipper electromagnetic and ground-based magnetotelluric data

GEOPHYSICS, VOL. 81, NO. 1 (JANUARY-FEBRUARY 2016); P. B1–B12, 12 FIGS.
10.1190/GEO2015-0230.1

Case History

Three-dimensional imaging of a Ag-Au-rich epithermal system in British Columbia, Canada, using airborne *z*-axis tipper electromagnetic and ground-based magnetotelluric data

Juliane Hübert[1], Benjamin M. Lee[2], Lijuan Liu[2], Martyn J. Unsworth[2], Jeremy P. Richards[2], Bahman Abbassi[3], Li Zhen Cheng[3], Douglas W. Oldenburg[4], Jean M. Legault[5], and Mark Rebagliati[6]

ABSTRACT

We have evaluated results from a study combining airborne *z*-axis tipper electromagnetic (ZTEM) and ground-based magnetotelluric (MT) data to image an epithermal system in British Columbia. The spatially coincident use of these two methods allowed for a direct comparison of both data sets in the overlapping frequency band and showed that both measurements were consistent. Inversion of just the ZTEM data suffered from the lack of electric field amplitude information, which could be provided by the MT data. Three-dimensional inversion modeling of the two individual data sets was performed. Models of electrical resistivity derived from both data sets were consistent and could be correlated with the geological and structural setting of the mineralization. Gold is associated with disseminated pyrite and marcasite in quartz-sericite-altered felsic volcanic rocks and intrusions, especially near the contact with mafic volcanic rocks and a late diorite intrusion. The quartz-sericite alteration yields a conductivity anomaly, relative to the more resistive mafic country rocks. Although ZTEM and MT do not possess the resolution of the geologic model derived from borehole data, our model agrees well with a regional assessment of the deposit.

INTRODUCTION

The techniques most commonly used for regional-scale mineral exploration are airborne geophysical methods, such as electromagnetic (EM) and magnetic surveys (Grant, 1985; Thompson, 1995; Cheng et al., 2006; Howe and Kroll, 2010). Airborne EM surveys have been successfully used to locate mineralized zones within exposed ore-forming systems, and they have proven particularly effective in identifying metal sulfide-rich ore bodies because of the mostly low electric resistivity of these minerals relative to typically resistive host rocks (Vallee et al., 2011). However, porphyry-Cu and related epithermal deposits generally exhibit only a modest contrast in electrical resistivity due to the lower abundance and disseminated distribution of the sulfide minerals. Additional field studies are needed to determine the most effective exploration approach for this

Manuscript received by the Editor 15 April 2015; revised manuscript received 21 September 2015; published online 22 December 2015.
[1]Formerly University of Alberta, Department of Earth and Atmospheric Sciences, Edmonton, Alberta, Canada; presently University of Edinburgh, School of Geosciences, Edinburgh, UK. E-mail: juliane.huebert@ed.ac.uk.
[2]University of Alberta, Department of Earth and Atmospheric Sciences, Edmonton, Alberta, Canada. E-mail: blee3@ualberta.ca; lijuan1@ualberta.ca; unsworth@ualberta.ca; jeremy.richards@ualberta.ca.
[3]Université du Québec en Abitibi-Témiscamingue, Département des Sciences appliquées, Rouyn Noranda, Québec, Canada. E-mail: bahman.abbassi@uqat.ca; li_zhen.cheng@uqat.ca.
[4]University of British Columbia, Department of Earth and Ocean Sciences, UBC Geophysical Inversion Facility, Vancouver, British Columbia, Canada. E-mail: doug@eos.ubc.ca.
[5]Geotech Ltd., Aurora, Ontario, Canada. E-mail: jean@geotech.ca.
[6]Amarc Resources Ltd., Vancouver, Canada. E-mail: markrebagliati@hdimining.com.

type of deposit (Oldenburg et al., 1997; Hoschke, 2008; Bournas et al., 2013).

The airborne *z*-axis tipper electromagnetic (ZTEM) technique (Lo and Zang, 2008; Legault et al., 2009) measures natural low-frequency (30–720 Hz) EM signals, and it is used for deep mineral exploration extending to depths of up to 2 km in ideal circumstances and resistive terrain, depending on the average electric resistivity of the area (Spies, 1989). The method is closely related to the ground-based magnetotelluric (MT) method, which also uses natural EM signals and has been applied to a wide variety of targets from near-surface to deeper mantle studies (Bastani et al., 2009; Bertrand et al., 2012; Rippe et al., 2013). MT measurements require contact with the ground and are thus relatively slow and expensive if large areas are to be explored. However, because the electric and magnetic fields are measured, MT can give estimates of the depth and horizontal position of a target, in addition to absolute resistivity values. In contrast to MT, ZTEM data can be collected from an airborne platform allowing rapid coverage of large areas including less accessible terrain. Only magnetic fields are measured to derive the ratio between vertical and horizontal magnetic field components, the so-called tipper. Tipper data possess good sensitivity to the horizontal location of low-resistivity targets, but they have poor to no resolution in the vertical direction. The lack of electric field data means that only variations in resistivity can be recovered and not absolute values. Therefore, MT and ZTEM can potentially complement one another, with ZTEM offering better spatial coverage and MT providing deeper images and absolute resistivity values. Recent studies investigating the applicability of synthetic ZTEM and MT data inversion are performed by Spratt et al. (2012) and Sasaki et al. (2014). Legault et al. (2011) and Legault and Wannamaker (2014) present joint inversions of MT impedance and ZTEM tipper data, but case studies with tipper data collected with both methods on the same target have not been published before.

In this paper, we present joint MT-ZTEM data from the Newton epithermal Au-Ag deposit in British Columbia, Canada, which is interpreted to represent the shallow part of a deeper porphyry Cu-type system. Porphyry and epithermal deposits represent a particular challenge for EM methods because the electrical resistivity contrasts between mineralized and unmineralized rocks can be quite small (approximately one order of magnitude). Interpretation of EM data therefore, requires an integrative approach, using additional constraints from other geophysical methods and known geology. This work was conducted as part of the project "Mineral Exploration under Deep Cover: Improving the Effectiveness of ZTEM Surveys for Porphyry Copper Exploration in the Canadian Cordillera," and it was a collaboration between several Canadian universities and industry partners.

PORPHYRY AND EPITHERMAL DEPOSITS — GEOPHYSICAL RESPONSES

Porphyry and related epithermal systems are closely associated with an underlying pluton, and the intrusive stocks or dikes and hydrothermal fluids derived from the pluton generate characteristic alteration styles and associated mineralization. Porphyry Cu ± Mo ± Au mineralization occurs as disseminations and veinlet networks (stockworks) containing chalcopyrite associated with potassic (K-feldspar-biotite) alteration in the deeper parts of the systems. Intermediate to high sulfidation (HS) epithermal Au ± Ag ± Cu mineralization associated with phyllic (quartz-sericite-pyrite), argillic (quartz-kaolinite), and advanced argillic (alunite-diaspore-kaolinite) alteration occurs at progressively shallower levels above the porphyry. The spatial relationships between alteration styles, mineralization, and expected geophysical signatures are illustrated in Figure 1. Typically, hydrothermal alteration (Figure 1b; potassic, phyllic, argillic, advanced argillic, and distal propylitic) form zones or occur as halos around the intrusion (Lowell and Guilbert, 1970; Sillitoe, 2010).

Porphyry deposits have distinct geophysical responses, as discussed by Ford et al. (2007) and investigated by Mitchinson et al. (2013) and these are illustrated schematically in Figure 1d–1f. The magnetic response is characterized by high susceptibility in the intrusion and the potassic zone due to the presence of igneous and hydrothermal magnetite (Figure 1d). However, hydrothermal alteration converts magnetite to pyrite in the phyllic zone, causing a strong decrease in magnetic susceptibility. The surrounding country rock typically has variable, intermediate susceptibility, depending on the lithology. Thus, porphyry systems are characterized by a central moderate magnetic susceptibility high, corresponding to the mineralized core of the system, surrounded by a distinct magnetic low (which may be annular if the system is undeformed), and a distal region of variable but generally higher magnetic susceptibility.

Electrical resistivity is high in fresh and potassic-altered intrusive rocks and can be high in the country rock as well. Phyllic- and argillic-altered rocks have lower electrical resistivity due to the abundance of conductive phyllosilicate minerals, such as sericite, muscovite, and clays. The presence of sulfide minerals can also decrease electrical resistivity. However, sulfides in porphyry deposits are mostly disseminated at relatively low concentrations (rarely more than a few volume percent) and thus do not cause significant resistivity reductions (Nelson and Vanvoorhis, 1983; Mitchinson et al., 2013). For example, at Mount Milligan, which is a well-studied porphyry Cu-Au deposit in British Columbia, a sulfide content of approximately 20% in propylitic altered rocks produced a minimum resistivity of just 10 Ωm, whereas sulfide contents of 1% in potassic altered rocks gave resistivities greater than 1000 Ωm. Resistivity will also be lower in the argillic zone due to the presence of clay minerals. Hypothetical profiles of resistivity for different erosion levels are shown in Figure 1e. Chargeability is high wherever there are elevated concentrations of sulfides. Thus, strong induced-polarization (IP) anomalies are associated with the pyritic phyllic alteration zone (which may contain a few tens of percent pyrite), whereas the potassic zone, which contains lower abundances of sulfide (mainly chalcopyrite and minor bornite), will give a lower response. This results in a characteristic annular chargeability high over the phyllic zone surrounding the center of the porphyry system, which coincides with the annular magnetic low described above (Figure 1f).

However, it should be stressed that these models are idealized, and the geometry of porphyry deposits is commonly disrupted by tectonic processes after mineralization has occurred, such that geophysical patterns require careful interpretation in the light of known geology. In the following, we present a comparative study of spatially coincident ZTEM and MT data from the undeveloped Newton epithermal Au-Ag deposit in central British Columbia, Canada (Figure 2). This target was chosen due to ground accessibility, which allowed the collection of MT data, access to a large

regional ZTEM survey over the deposit area, and the availability of geologic information from the drill core. The exposed part of the Newton deposit has been classified as an intermediate-sulfidation epithermal deposit, but there are indications in the drill core that it is underlain by a porphyry deposit (McClenaghan, 2013; L. Liu, personal communication, 2015). Geophysical, geological, and geochemical exploration in the area has been conducted since the 1970s by several companies and include ground-based DC resistivity and IP measurements (Pressacco, 2012). The most recent drilling program from 2009 to 2012 was conducted by Amarc Resources Ltd., and comprised 89 diamond drillholes with a total length of 27,944 m.

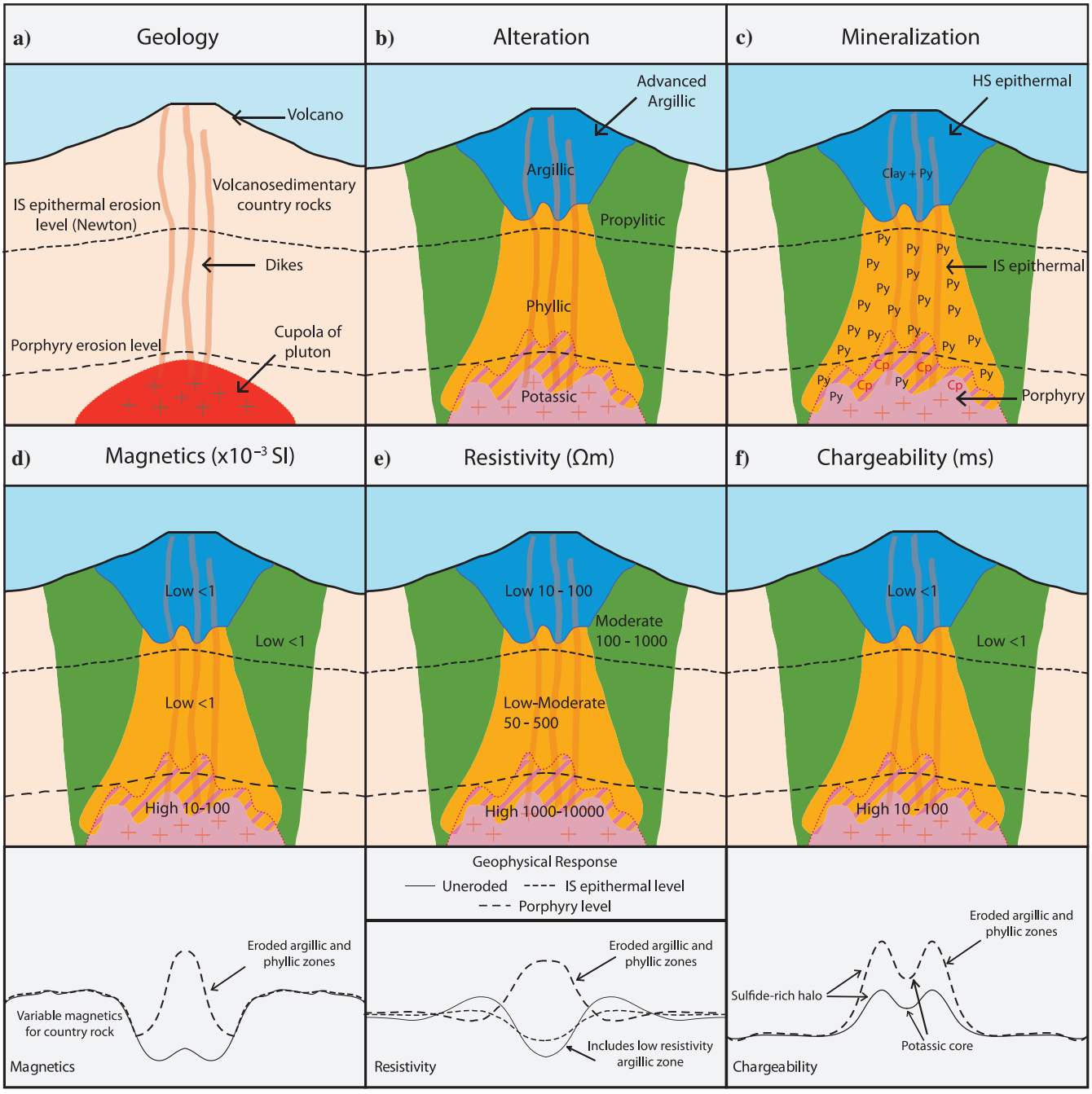

Figure 1. Schematic representation of an epithermal-porphyry system with petrophysical properties. (a) Geologic cross section with the suggested present-day surface at two possible levels of erosion. (b) Location of alteration styles common for porphyry and epithermal systems. (c) Mineralization styles associated with porphyry, intermediate sulfidation epithermal (IS), and high sulfidation (HS) epithermal deposits. (d-f) Expected magnetic susceptibility, electric resistivity, and chargeability responses over the eroded and uneroded system. Based on the models of Lowell and Guilbert (1970), Sillitoe (2010), and petrophysical values of Mitchinson et al. (2013). Abbreviations: Cp, chalcopyrite and Py, pyrite.

GEOLOGY AND TECTONIC SETTING OF THE NEWTON DEPOSIT

The Canadian Cordillera in British Columbia is composed of distinct terranes, including ancient passive continental margin, island arcs, and accretionary wedges. It hosts significant porphyry and epithermal deposits (McMillan et al., 1995; Nelson and Colpron, 2007), such as the Highland Valley porphyry Cu-Mo deposit, Galore Creek porphyry Cu-Au-Ag deposit, Endako porphyry Mo deposit, Prosperity porphyry Cu-Au deposit, Toodoggone epithermal Au-Ag deposit, Blackdome epithermal Au-Ag deposit, and the Capoose epithermal Au-Ag deposit. The Newton epithermal Au-Ag deposit (Figure 2) is located in the southern Stikinia terrane, within the Intermontane belt of central British Columbia (Monger and Price, 2002). The deposit is owned by Amarc Resources Ltd., which has delineated an inferred resource of 111.1 million tonnes with an average grade of 0.44 g/t gold and 2.1 g/t silver; Cu is also locally present up to 0.2% but is not part of the resource. It is genetically and spatially associated with Late Cretaceous calc-alkaline felsic volcanic rocks and associated intrusions (Bordet et al., 2011) and is situated between two regional dextral strike-slip faults: the Yalakom fault to the west and the Fraser fault to the east (Figure 2). Quaternary glacial till covers most of the Newton property, and outcrops are sparse; consequently, geologic information has primarily been obtained from drill cores (Figure 3).

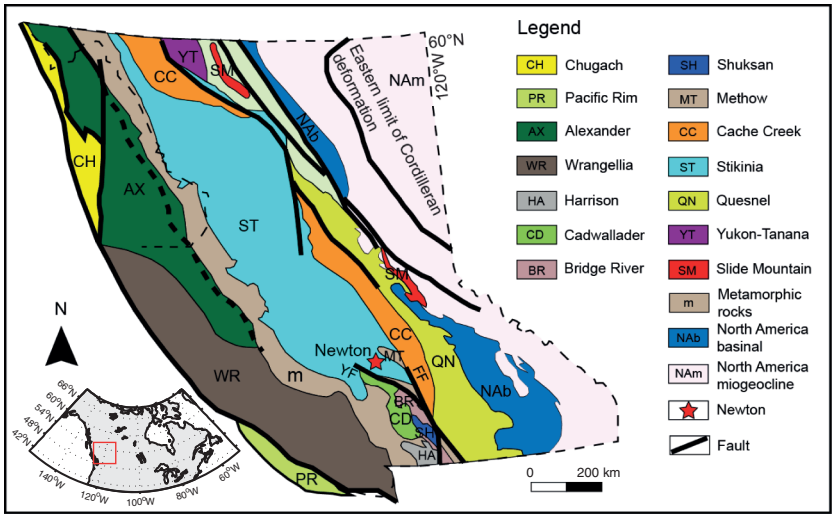

Figure 2. Terrane map of the British Columbian Cordillera, showing the location of the Newton Au-Ag deposit (red star) in the southern Stikinia terrane. Modified from Nelson and Colpron (2007).

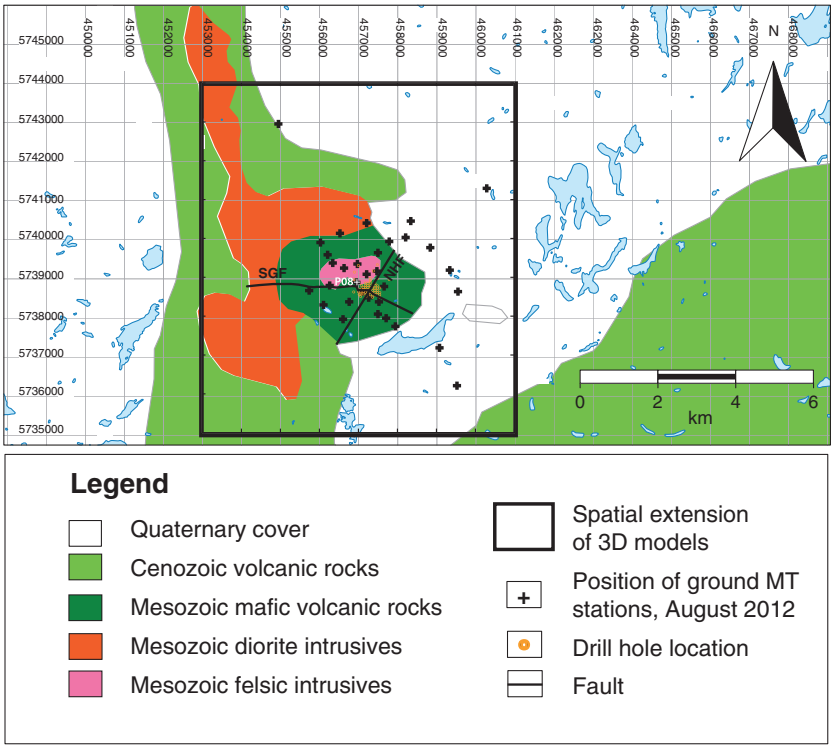

Figure 3. Regional geologic overview of the Newton area with locations of MT stations, modified after British Columbia Geological Survey Geoscience Map (mapplace.ca). Map coordinates are in UTM, zone 10, and NAD 83.

The Newton deposit is characterized by three main lithological units: Late Cretaceous mafic and felsic volcanic rocks, sedimentary rocks, and intermediate to felsic plutonic rocks (diorite, granodiorite, and quartz-feldspar porphyry; Figure 3). Undated mafic volcanic rocks are considered to be the oldest unit in the area, and have basaltic to andesitic compositions. These are overlain by Late Cretaceous felsic volcanic rocks (rhyolitic tuffs), which form the primary host rock for the mineralization at Newton. The felsic volcanic rocks formed at 72.1 ± 0.3 Ma, and the quartz-feldspar porphyry has been dated at 70.9 ± 0.5 Ma (unpublished zircon U-Pb analysis, Amarc Resources Ltd., reported in McClenaghan, 2013). The diorite is the youngest intrusive phase (69.07 ± 0.52 Ma; L. Liu, personal communication, 2015); it is unmineralized and is the least altered unit. Sedimentary rocks, consisting mainly of conglomerates, mudstones, and sandstones, occur to the east of the deposit, and stratigraphically overlie the mafic volcanic rocks.

Several faults have been identified around the Newton property, the most prominent being the postmineralization Newton Hill Fault (NHF), which cuts through the mineralized zone with a strike of approximately 27° and a dip of approximately 30° to the northwest. The fault displays 300–350 m of normal displacement (Pressacco, 2012). The mineralized zone is located below the top of Newton Hill, which is the highest point in the area, rising approximately 150 m above the surrounding land. Hydrothermal alteration affects all rock types to varying degrees. Pervasive phyllic (quartz-sericite) alteration is found in the felsic volcanic rocks, whereas propylitic alteration (chlorite, epidote, and calcite) is developed

in the mafic volcanic rocks and more weakly in the late diorite intrusion. Potassic alteration (K-feldspar and biotite, lacking significant Cu $\pm$ Mo $\pm$ Au mineralization at the depths explored to date) is locally present in the diorite. Argillic alteration is weak and only locally present in the felsic volcanic rocks; this type of alteration may represent a late overprint (L. Liu, personal communication, 2015).

The gold mineralization at Newton is closely related to the quartz-sericite alteration, which mainly occurs in the felsic volcanic rocks, the quartz feldspar porphyry, and the granodiorite. The quartz-sericite-altered rocks host abundant disseminated pyrite and marcasite, in which gold is present as electrum and gold-silver telluride inclusions. Additionally, polymetallic veins (mainly containing sphalerite and galena) occur in the sedimentary rocks and the felsic volcanic rocks. They are not common and are considered to have formed later than the Au mineralization. Geologic data from the logs of 130 drill cores (locations in Figure 4) from a localized area around the deposit were available for analysis. Based on this lithological data and several geological cross sections (courtesy of Amarc Resources Ltd.), a 3D geologic model extending 2×2 km around the deposit was constructed with the help of the software suite Paradigm GOCAD®, to a maximum depth of 0.6 km below the surface. The planes of the NHF and South Graben Fault (SGF) were implicitly modeled from observations in the drill cores.

GEOPHYSICAL METHODS AND DATA COLLECTION

MT and ZTEM

The ZTEM method shares a theoretical background with MT, using the same natural electromagnetic field variations generated in the ionosphere and by global lightning to image the electrical resistivity structure of the subsurface. The penetration depth depends on the frequency of the measured signal according to the skin depth equation, with higher frequencies (up to 720 Hz) probing the shallower subsurface (<0.6 km) and lower frequencies (usually approximately 30 Hz) penetrating to depths of $\leq$2 km (for background resistivities >500 Ωm). The receiver, a horizontal airborne coil mounted on a bird towed below a helicopter, measures the vertical magnetic field component, whereas two coils at a ground base station measure the horizontal field components. An additional sensor towed beneath the aircraft measures the total magnetic field. This method was first proposed in the 1950s by Ward (1959), and it was then called the audio-frequency magnetic (AFMAG) method. It was developed through the 1980s (Labson et al., 1985), but technological advances minimizing electric noise from the aircraft and enabling the monitoring of sensor position have only recently allowed large, high-quality data sets to be collected. Applications have included base metal and unconformity uranium

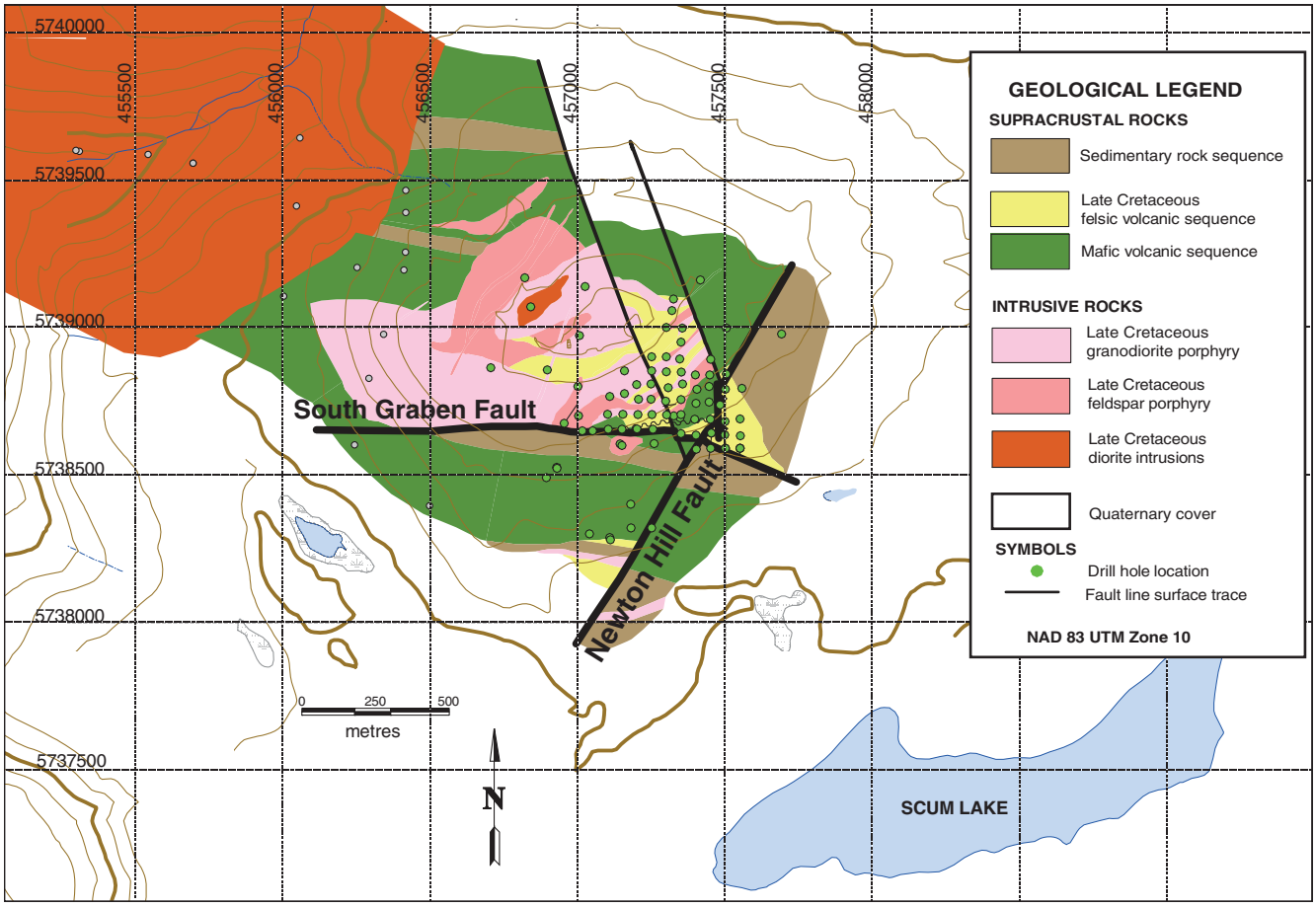

Figure 4. Geologic map of the Newton deposit. Modified after McClenaghan (2013).

exploration (Lo and Zang, 2008; Legault et al., 2009), as well as geothermal exploration (Devriese et al., 2012). The 2D and 3D inversion techniques developed for MT or controlled-source airborne methods (Siripunvaraporn and Egbert, 2009; Holtham and Oldenburg, 2010; Egbert and Kelbert, 2012) can be applied to ZTEM data to derive models of electric resistivity. The ground-based tipper is estimated from MT time series recordings at discrete frequencies ω at a location r as the complex quantity T, and it includes measurements of the horizontal components of the magnetic field at a base station r_0 (Vozoff, 1991):

$$H_z(r,\omega) = T_{zx}(r,\omega)H_x(r,\omega) + T_{zy}(r,\omega)H_y(r,\omega), \quad (1)$$

whereas the airborne tipper of ZTEM is described through

$$H_z(r,\omega) = T_{zx}(r,r_0,\omega)H_x(r_0,\omega) + T_{zy}(r,r_0,\omega)H_y(r_0,\omega). \quad (2)$$

The time variations of the vertical magnetic field H_z are recorded with a helicopter-towed bird at a height of approximately 80 m above the ground.

During January and February 2010, Geotech Ltd. carried out a helicopter-borne geophysical survey for Amarc Resources Ltd. over the Newton property, comprising ZTEM and aeromagnetic measurements along 36 north–south-directed flight lines with horizontal spacing of 200 m and along-line sampling of 12 m as part of a larger block extending to the east and south of the ground exploration area (the black frame in Figure 3). The recorded ZTEM data were processed at five selected frequencies (30, 45, 90, 180, and 360 Hz) by Geotech (Geotech Ltd., 2010) and were provided together with topographic information as well as exact GPS locations and bird heights.

In August 2012, 33 MT ground stations were installed around Newton Hill by a team from the University of Alberta with assistance from Peter E. Walcott & Associates Limited in a relatively dense grid (the minimum site spacing was 250 m) around the mapped deposit on Newton Hill. Each MT installation recorded five channels of data with a Phoenix V5-2000 system. This consisted of two horizontal electric fields with 100 m dipoles and three components of the magnetic field. The MT data quality was high despite the short recording times (6 h of daytime data or 12 h of nighttime recording), indicating sufficient

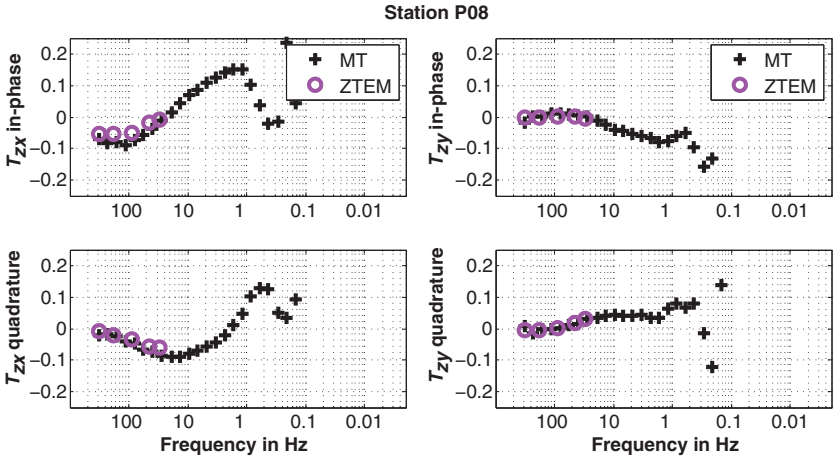

Figure 5. Comparison between tipper data measured with ground MT (black crosses) and airborne ZTEM (purple circles) at MT site P08 (location shown in Figure 3). Each subplot shows one of the four components of the complex tipper vector. The data show excellent agreement in the frequency range of overlap.

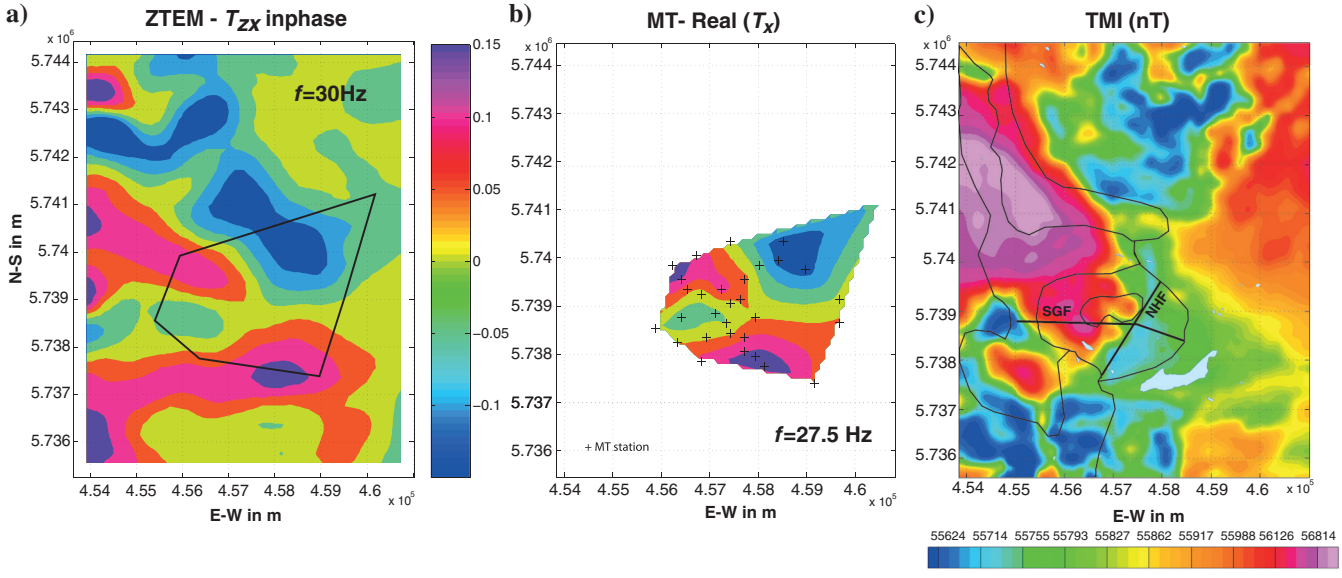

Figure 6. Comparison of tipper data one component, T_{zx} in-phase/real part, $f = 30$ Hz for the (a) ZTEM and (b) MT ($f = 27.5$ Hz) data sets in map view. Coordinates are in UTM. The black polygon in the ZTEM panel indicates the spatial coverage of the MT data for reference. (c) Total magnetic field intensity over the deposit as measured by Geotech. The black lines indicate faults at the surface and the outline of the main lithological units from Figure 3.

signal strength in the audio-MT frequency range. The recorded time series were processed into impedance and tipper data in the frequency range 320–0.001 Hz using simultaneously recording sites as a remote reference. This allowed for a direct comparison between the airborne and ground tipper data in the frequency band at which the two techniques overlap and showed an excellent agreement between the two data sets (Figure 5). The data were also well correlated spatially (Figure 6) despite the different altitudes and sensors used in the two methods (the induction coils for the MT measurements were buried at a depth of 30 cm, whereas the air coil of the ZTEM system was towed at approximately 80 m above the ground). The bird altitude was monitored with radar, whereas the elevation of the MT sites was estimated from the digital elevation model provided by GeoBase, an initiative overseen by the Canadian Council on Geomatics.

Airborne magnetic data

Aeromagnetic data were collected at the same time as the ZTEM data, using a Geometrics split-beam, optically pumped, cesium vapor magnetic field sensor (Geotech Ltd., 2010). This was mounted on a separate bird, and it recorded the total magnetic field intensity (Figure 6c). The most prominent feature is the positive magnetic signature of the diorite intrusion, which is truncated by the NHF in the southeast. Work in progress includes the 3D inversion of the magnetic data including constraints from petrophysical measurements on the drill cores. This work will provide an indication of mineral assemblages at depth.

3D inversion of ZTEM and MT data

The ZTEM and MT data were inverted to determine a 3D model of electrical resistivity using the Gauss-Newton-type algorithm e3dMTinv of Holtham and Oldenburg (2010). The model discretization used an octree approach (Yang and Oldenburg, 2012), which is an improvement on regular rectangular meshes because it significantly reduces the number of cells needed in the inversion to represent the subsurface resistivity by combining cells outside the observation area into larger cells (Figure 7). This drastically reduces the problem size and computer memory needed and therefore the time and memory requirements of the computation. In this study, the number of cells and therefore model parameters were reduced by three orders of magnitude from 3×10^8 to 4×10^5 cells for the chosen cell size for the core region of $50 \times 50 \times 25$ m.

The model discretization accounted for topography, which was extracted from the digital elevation model. The influence of topography can be studied by investigating the tipper response of a half-space model, which is nonzero for a nonflat surface. The largest elevation difference is in the southwest corner of the study area, where the relief drops into the valley of the Taseko River (1050 m above sea level), which is a visible effect in the tipper data. The highest elevation is Newton Hill (1330 m), which gently rises on average approximately 150 m above the surrounding area (see Figure 7c).

For the ZTEM data inversion, all 26,000 data points per frequency were used. We tested different minimum cell sizes and background resistivities. It was also necessary to estimate the standard deviations in the data because no error estimates for the ZTEM data were provided. Assigning appropriate data errors is essential to produce a balanced fit of all data components and frequencies (Holtham and Oldenburg, 2010). The ZTEM data were assigned a combination of an absolute error of 0.005 plus a relative percentage error of 5% of each component of the tipper. During model discretization in 3D, the choice of the mesh is restricted by the substantial computational costs because even modern multiprocessor facilities have limited memory resources (the chosen model required 17 GB of RAM per node).

A series of tests with a reduced ZTEM data set (one frequency block at a time) using different background resistivities was performed. The analysis illustrates that tipper data in 3D are sensitive to the absolute resistivity, due to the topographic effect, which results in a nonzero response of a homogeneous half-space subsurface (Figure 8). Using a higher background resistivity of 1000 Ωm resulted in much slower convergence of the inversion problem. Lowering the background resistivity from 100 to 50 Ωm did not improve

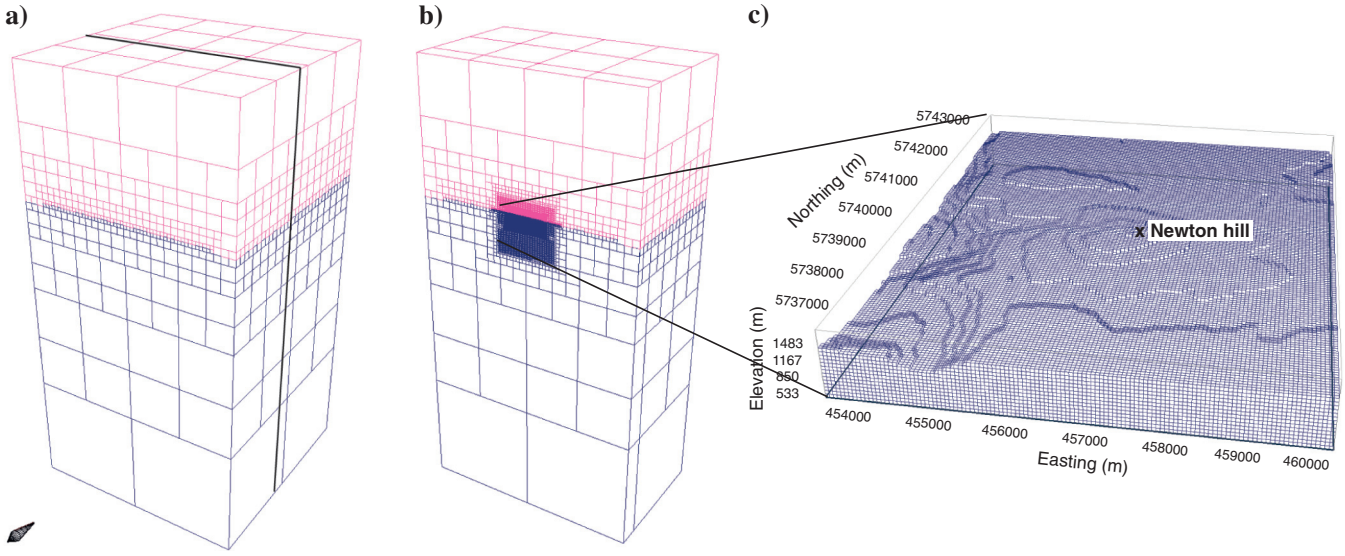

Figure 7. Model mesh with octree discretization. (a) Complete model with air cells (red). (b) Fine discretization in the center area. (c) Topography around the Newton deposit.

the convergence significantly. Eventually, a homogeneous half-space of 80 Ωm was used to derive a model with similar resistivity amplitudes to the MT model. This background resistivity was also in good agreement with existing DC resistivity models provided by Amarc Resources Ltd. for comparison, which showed an average background resistivity in the range 80–120 Ωm in the upper 500 m. The inversion algorithm is parallelized over frequencies, and computations were performed on multiprocessor clusters operated by WestGrid. Inversion runs were performed on as many processors as frequencies used (five for ZTEM and 17 for MT) and took several days before converging. For the inversion of MT data, the impedance data (all four components) at 17 frequencies between 1 and 320 Hz were used. The assigned errors were the sum of an error floor of 3% of the impedance main components (Z_{xy} and Z_{yx}) and 5% Gaussian noise per data point, following the approach of Holtham and Oldenburg (2010). The same error floor was used for the corresponding diagonal component (e.g., $\text{errfl}(Z_{xx}) = \text{errfl}(Z_{xy})$). In the single ZTEM and MT inversions, the derived models were able to fit the data within the error bounds. Examples of the data fit can be seen in Figure 9 for ZTEM and Figure 10 for MT data.

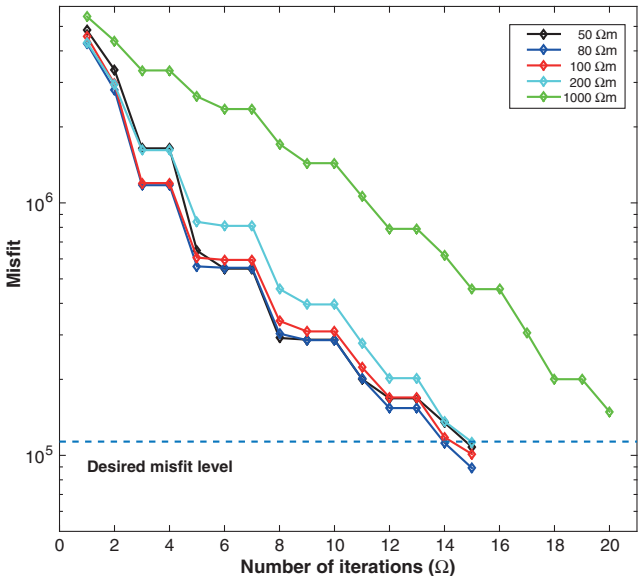

Figure 8. Convergence for five different starting models/resistivity backgrounds using the 30 Hz subset of the ZTEM data and a cell size of $50 \times 50 \times 50$ m in the core region. The dashed line represents the desired misfit level, corresponding to a rms of one within the chosen error bounds.

Joint inversion of the two data sets was attempted using the inversion algorithm of Holtham and Oldenburg (2010), which was designed to invert impedance and tipper data simultaneously. In their approach, multiple data blocks can be inverted that contain different frequencies, station locations, and data types. A balanced data fit, which in this case is the most difficult part of the joint inversion, has to be controlled with data weighting through the assignment of modified standard deviations. However, due to the irregular spatial distribution of MT sites, it is difficult to find a satisfactory weighting that produced a model that equally explained the ZTEM and MT data. Efforts are still ongoing to find an appropriate weighting scheme, and the results of joint inversion will be the subject of a future publication.

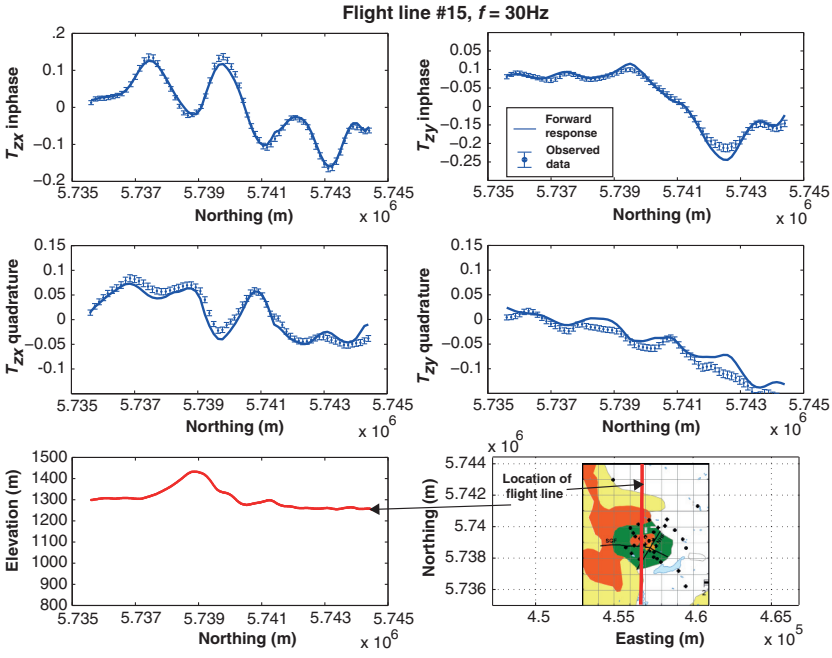

Figure 9. Measured (circles with error bars) and forward data (solid line) for one flight line across the deposit for ZTEM tipper data at 30 Hz. Along the flight lines sampling is 12 m. For this figure, ZTEM data points were downsampled for visualization only. All data points were used in the inversion. The position and elevation across the flight line are displayed in the lower panels. For the legend of the geologic map, see Figure 3.

Resistivity models

The electrical resistivity models derived from the inversion of the two data sets generally show similar features and resistivity amplitudes. Resistivities vary over two decades from 10 to 300 Ωm. The MT model (Figure 11a–11c) suffers from spatial bias due to the irregular distribution of stations, which were centered closely around the Newton deposit. The near-surface parts of the model (the first few layers up to approximately 100 m depth at 1070 m elevation; Figure 11a) are controlled by small surface distortions and the regularization. Below that depth, the model becomes spatially smoother. There are conductive regions in the center, northeast, and southwest parts of the model (labeled C1–C3, respectively in Figure 11). The central conductor C1 is enclosed by a more resistive ring (R1), which extends to about 600 m depth (Figure 11c). A resistive zone extends from the near surface to depth in the northwest part of the model (R2 in Figure 11), and it is connected to R1 in the deeper part of the model. Model features located outside the area of observation below depths greater than 1 km (elevation below 500 m) are not resolved, meaning that the extent of C2, C3, and R2 cannot be inferred, even though their presence is required by the data.

The ZTEM model (Figure 11d–11f) does not suffer from the spatial bias of the impedance model in the shallow subsurface, and it resolves lateral resistivity changes well due to the very regular spatial sampling along the flight lines of the survey. The absolute resistivity values in the model match those of the MT model. This was achieved by choosing a background resistivity of 80 Ωm during the inversion as a priori information from the MT data. Most prominent is the large resistive body (labeled R1 in Figure 11d–11f) that extends from the center of the study area to the northwest (linking with R2, as seen in the MT model), and bordered to the northeast by a conductive zone (C2, as also seen in the MT model). The central conductor C1 is resolved slightly more to the west (1–2 km) compared with the MT model.

Below a depth of approximately 700 m (at elevation 500 m; see Figure 11c and 11f), the resolution of both the models decreases and the model features are smoothed out. The lateral resolution of the electrical resistivity anomalies in the upper kilometer of both models appears to be mainly controlled by the data coverage. MT stations were concentrated around the known location of the mineralization; therefore, the MT model is spatially biased in the outer areas with less data coverage. ZTEM data were collected with much denser spatial coverage, and the resulting model has high lateral resolution everywhere inside the modeling domain. Accordingly, the ZTEM model shows more detail at the surface (Figure 11d), and the image of the outer parts of the model is more reliable than in the MT model. Vertical resolution below 700 m is

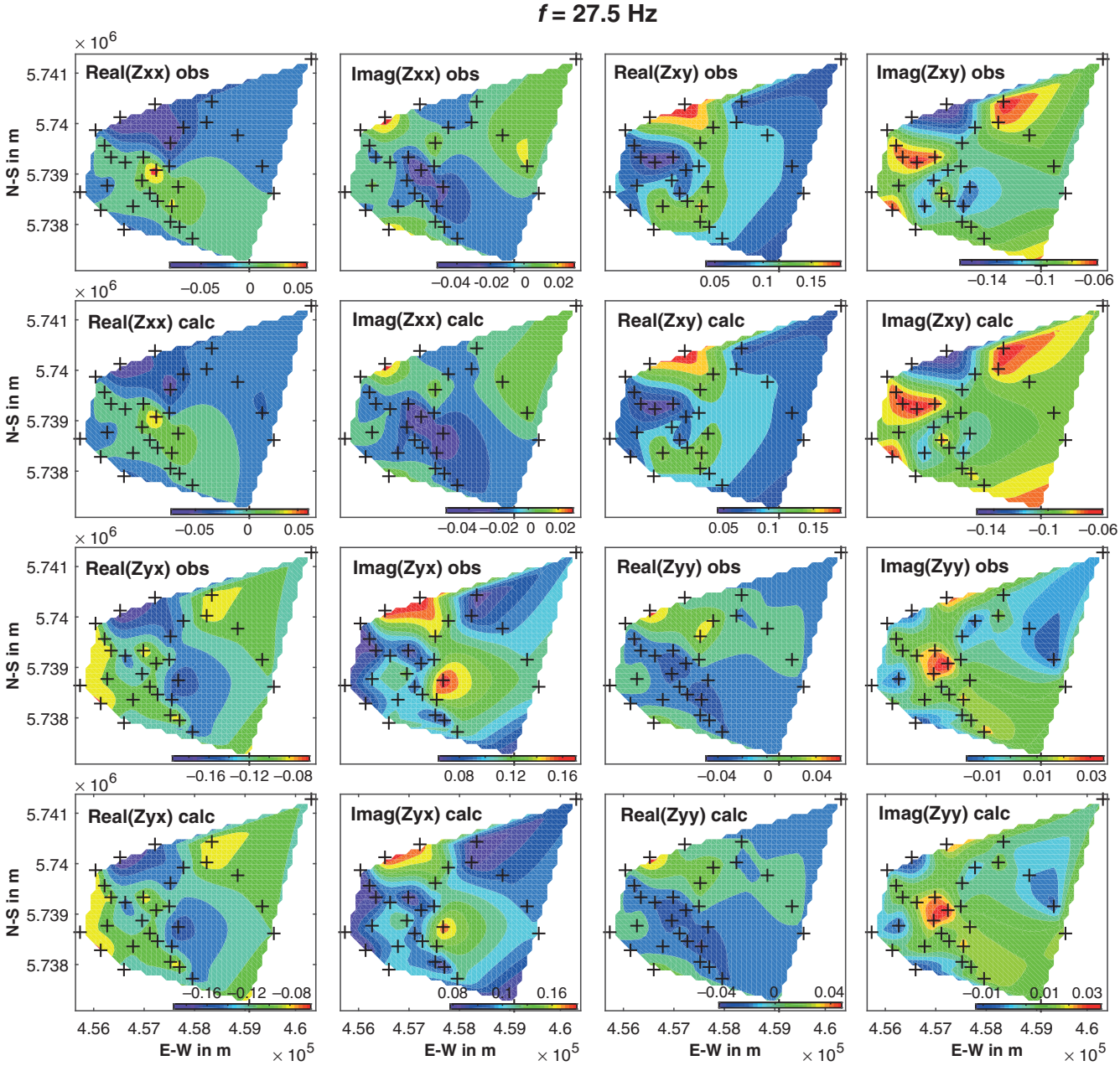

Figure 10. Map view of observed and forward data computed from the model presented in Figure 11 for all eight MT impedance tensor components at 27.5 Hz.

restricted for the ZTEM modeling by the frequency range, and it is limited by the small aperture of the station array for MT. Generally, lateral variations in resistivity can only be resolved up to a depth of the order of magnitude of the aperture of the measurement array.

INTERPRETATION

Comparing geophysical models to geological observations often results in the problem of comparing features with very different spatial scales. Although the resolution of the ZTEM model does not support a direct comparison with the more detailed geologic observations, it is possible to infer spatial correlation between the lithological units and their alteration stages and the electric features.

The eastern edge of the central conductor C1 (in Figures 11 and 12) is coincident with the array of drill holes shown in Figure 4 that identified the mineralized zone. The location of C1 coincides with the felsic volcanic and porphyry intrusive rocks. The MT inversion model shows that C1 has a resistivity in the range of 10–100 Ωm from the surface to a depth of approximately 700 m (Figure 11a–11c). These units have undergone quartz-sericite (phyllic) alteration, and the low electric resistivity could therefore be attributed to the presence of phyllosilicate minerals produced by alteration. Mitchinson et al. (2013) also suggest that alteration can raise the porosity and if the pore space is filled with aqueous fluids, this would also contribute to the low resistivity. The presence of two faults enveloping the central conductor C1 (Figure 12) could also favor an increase in porosity in these units. Additionally, some contribution to the lowered resistivity originates from the sulfide mineralization itself. McClenaghan (2013) reports a sulfide content of 2%–7% in the felsic volcanic sequence. Based on studies of related porphyry deposits in British Colombia with disseminated sulfides (Mitchinson et al., 2013), this concentration of sulfide corresponds to resistivities greater than 100 Ωm. Thus, the disseminated sulfide mineralization alone cannot account for the observed resistivity.

The mafic volcanic and the diorite intrusive rocks, which have mainly only undergone propylitic alteration, are associated with zones of higher resistivity (R1 and R2 in Figures 11 and 12), which extend from the northwest to the center of the study area, and they surround the central conductor C1.

The glacial till cover to the north and the area around the lake in the south of Newton Hill (Figures 3 and 4) are imaged as less resistive features (C2 and C3 in Figure 11), which can be explained by higher porosity and the presence of pore fluids and clays in these young, unconsolidated sediments. The amplitude of electrical resistivity as seen in conductors C1 and C2 is comparable with those associated with the altered felsic volcanic and porphyry rocks (C1). The depth extent of the glacial till is not resolved. Although numerous authors assume that a depth of investigation of 1.5 skin depths can be achieved, we assume the more conservative value of one skin depth. Therefore, a minimum depth extent of approximately 200 m can be estimated for the glacial till assuming a resistivity of 5 Ωm and the lowest frequency of the ZTEM data (30 Hz). Below this unit, there is no resolution in the deeper parts of the model (see shaded areas in Figure 11f).

The electrical resistivity model of the Newton property images the phyllic-altered rocks that host the mineralization as less resistive than the surrounding propylitic-altered rocks. This

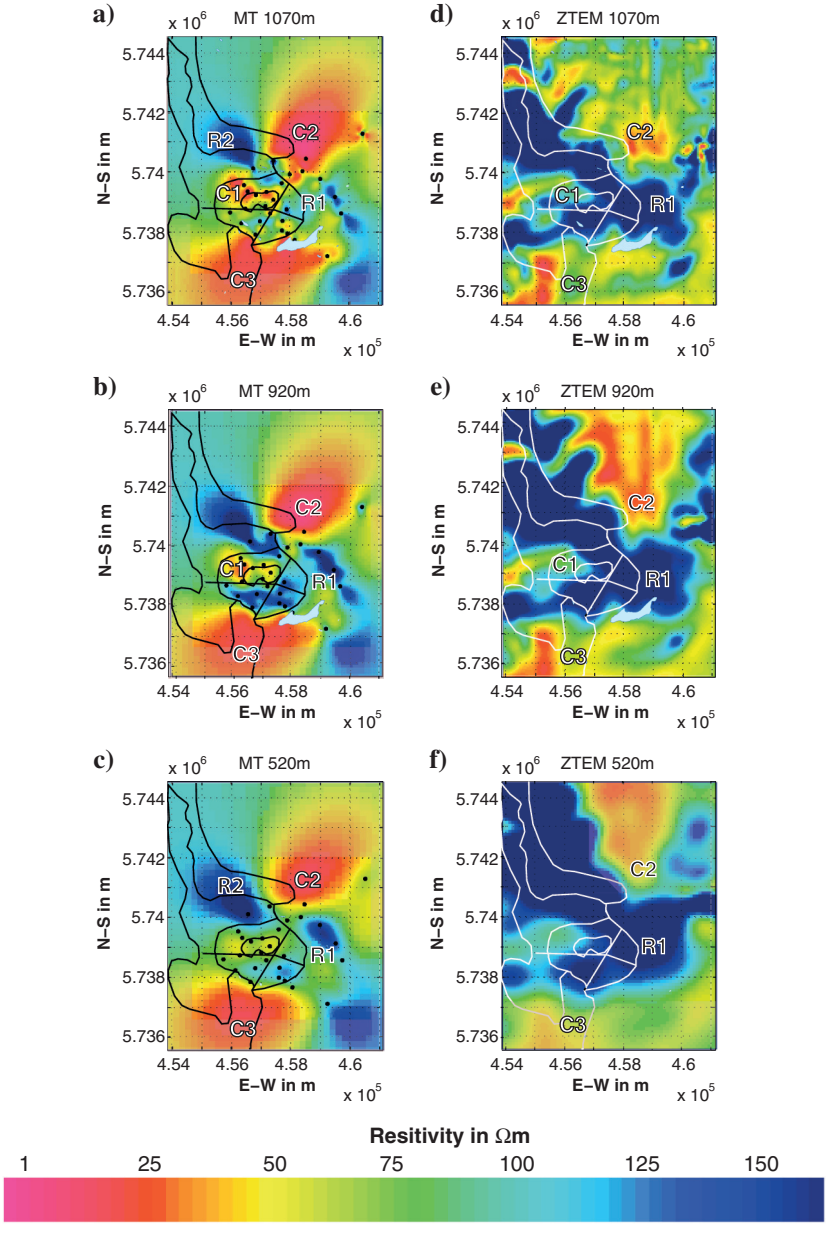

Figure 11. Electric resistivity models, estimated from MT impedance (left column, a-c) and ZTEM tipper data (right column, d-f) inversion for three different elevations. The average surface is at 1220 m. The letters refer to model features described in the text. The shaded areas indicate regions with no resolution. The black and white lines indicate faults at the surface and the outline of the main lithological units from Figure 1.

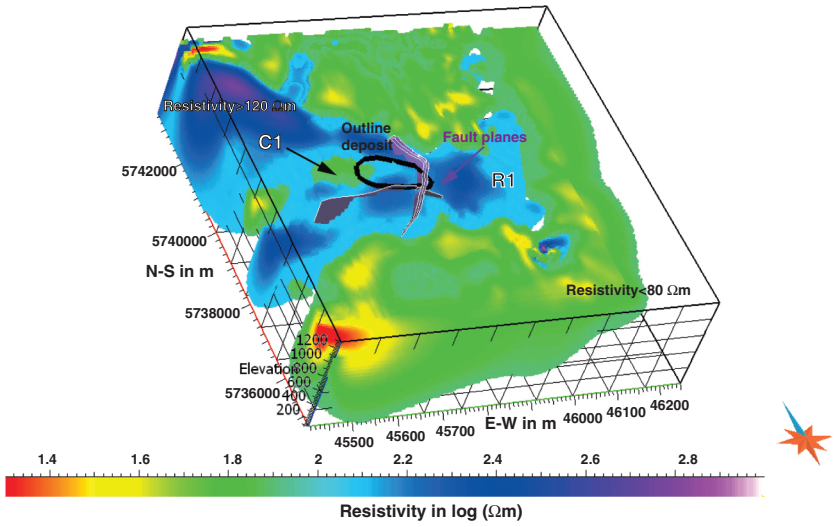

Figure 12. Electric resistivity model from ZTEM data shown as a 3D volume with two isosurfaces (conductors with $\rho < 80$ Ωm and resistors with $\rho > 120$ Ωm, displayed together with the planes of the Newton Hill Fault and South Graben Fault, which were modeled from boreholes, and the estimated outline of the deposit. The vertical exaggeration equals two. The main electric features C1, the conductor associated with the alteration, and R1, the mafic volcanic ricks and diorite instrusion, are labeled.

is in agreement with the conceptual model of a porphyry/epithermal system as presented in Figure 1e for an erosion level below the argillic zone. There are implications from geochemistry (fluid inclusions hint at the presence of higher temperature, halite-bearing fluids; L. Liu, personal communication, 2015) that an underlying porphyry system might exist below the mineralization at the Newton deposit. The associated expected zone of higher resistivity is not imaged by the presented ZTEM and MT models. This is likely due to the limited depth penetration of the ZTEM data and the small aperture of the MT station array. An electrical resistivity model with higher depth resolution could be achieved by several additional MT stations in a larger area around the deposit to increase the resolution aperture.

CONCLUSIONS

This is the first study to show in a case history that the vertical magnetic field data collected in a ZTEM survey are very similar to the vertical fields measured in conventional ground-based MT. Inversion allows resistivity models to be derived from the ZTEM data, which do not suffer from the spatial aliasing that arises from the nonuniform station coverage in the MT data. ZTEM data can easily image the electrical structure in relatively high resolution and to greater depths than DC resistivity studies. At Newton, the ZTEM electrical resistivity model images the major lithological units, especially the resistive mafic volcanic rocks and intrusive diorite and a conductive region associated with the hydrothermal alteration. The zone of mineralization is located at the edge of this conductive core comprising altered felsic volcanic and porphyritic rocks, bordered by two fault zones, which were implicitly modeled from borehole data. The epithermal-type deposit at Newton exhibits a modest electrical response (a factor of 10 variation in contrast to much higher amplitudes for sulfide deposits) relative to the resistivities of the surrounding country rocks, and this is mainly due to the presence of phyllosilicate minerals (sericite) and minor disseminated sulfides. The Quaternary cover has resistivities similar to the altered volcanic rocks that host the mineralization, likely due to its high porosity and water content, as well as the presence of clay minerals. The comparison of models from single MT and ZTEM data inversion is somewhat challenging due to the different spatial sampling and depth penetration, but both methods image electric features with comparable locations and resistivity values. For the exploration of porphyry and epithermal-type deposits, ZTEM delivers reliable 3D models of the subsurface, which are of comparable quality with ground-based methods but are much quicker to obtain. The direct correlation between mineral assemblages and geophysical response is ambiguous and needs to be constrained by spatial lithologic information derived from ground observations, ideally from boreholes. Together with the results of other geophysical techniques, a comprehensive picture of this ore deposit type can be obtained. The value of the MT data is that it provides a priori information about the absolute values of the electric resistivity, which can enhance the ZTEM inversions and provide 3D models to a greater depth than ZTEM data alone. Work in preparation includes the analysis of airborne magnetic and ground resistivity data together with borehole assays, geochemical data (radiometric gamma ray), and petrophysical measurements (magnetic susceptibility), to perform constrained inversions.

ACKNOWLEDGMENTS

This is part of an NSERC-funded research collaboration between the University of Alberta, l'Université du Québec en Abitibi-Témiscamingue, the University of British Columbia, Amarc Resources Ltd., Geotech Ltd., and Gerald G. Carlson and John A. Chapman. Amarc Resources Ltd. provided the ZTEM data. J. H. wishes to acknowledge the funding support by Geotech. Peter E. Walcott & Associates Limited and Mitchell Lidell are thanked for in-field assistance. Nicolas Pailot-Bonneta is thanked for implementing the geologic model in GOCAD. G. Rosenkjær and R. Shektman helped with the UBC code. This research was enabled in part by support provided by WestGrid and Compute Canada Calcul Canada. Two anonymous reviewers are thanked for their comments and suggestions that improved this paper.

REFERENCES

Bastani, M., A. Malehmir, N. Ismael, L. Pedersen, and F. Hedjazi, 2009, Delineating hydrothermal stockwork copper deposits using controlled-source and radio-magnetotelluric methods: A case study from northeast Iran: Geophysics, **74**, no. 5, B167–B181, doi: 10.1190/1.3174394.

Bertrand, E. A., T. G. Caldwell, G. J. Hill, E. L. Wallin, S. L. Bennie, N. Cozens, S. A. Onacha, G. A. Ryan, C. Walter, A. Zaino, and P. Wameyo, 2012, Magnetotelluric imaging of upper-crustal convection plumes beneath the Taupo Volcanic Zone and its hydrothermal circulation: Geophysical Research Letters, **39**, L02304, doi: 10.1029/2011GL050177.

Bordet, E., C. Hart, and L. McClenaghan, 2011, Epithermal-style-Au-Ag mineralization in Cretaceous to Eocene felsic volcanic complexes, central British Columbia, western Canada: Society for Geology Applied to Mineral Deposits.

Bournas, N., E. Clements, and R. Hearst, 2013, Discovery of polymetallic porphyry at the Silver Queen, British Columbia, using airborne EM and

TITAN-24 DCIP and MT surveys: Interpretation, **1**, no. 1, T101–T112, doi: 10.1190/INT-2013-0044.1.
Cheng, L., R. S. Smith, M. Allard, P. Keating, M. Chouteau, J. Lemieux, M. A. Vallée, D. Bois, and D. K. Fountain, 2006, Geophysical case study of the Iso and New Insco Deposits, Québec, Canada. Part II: Modelling and interpretation: Exploration and Mining Geology, **15**, 65–74, doi: 10.2113/gsemg.15.1-2.65.
Devriese, S., D. Oldenburg, and J. D. Shoffner, 2012, Three-dimensional inversion of ZTEM data at the Elevenmile Canyon Geothermal System, Nevada: GRC Transactions, **36**, 995–999.
Egbert, G., and A. Kelbert, 2012, Computational recipes for electromagnetic inverse problems: Geophysical Journal International, **189**, 251–267, doi: 10.1111/j.1365-246X.2011.05347.x.
Ford, K., P. Keating, and M. Thomas, 2007, Overview of geophysical signatures associated with Canadian ore deposits, *in* Goodfellow, W. D., ed., Mineral deposits of Canada — A synthesis of major deposit-types, district metallogeny, the evolution of geological provinces, and exploration methods 5: Geological Association of Canada, Mineral Deposits Division, 939–970.
Geotech Ltd., 2010, Report on a helicopter-borne Z-axis tipper electromagnetic (ZTEM) and aeromagnetic geophysical survey: Technical report, 10005/10016.
Grant, F. S., 1985, Aeromagnetics, geology and ore environments. 1: Magnetite in igneous, sedimentary and metamorphic rocks — An overview: Geoexploration, **23**, 303–333, doi: 10.1016/0016-7142(85)90001-8.
Holtham, E., and D. W. Oldenburg, 2010, Three-dimensional inversion of ZTEM data: Geophysical Journal International, **182**, 168–182.
Hoschke, T., 2008, Geophysical signatures of copper-gold porphyry and epithermal gold deposits: Ores and orogenesis: Circum-Pacific tectonics, geologic evolution, and ore deposits: Arizona Geological Society Digest, **22**, 85–100.
Howe, B., and A. Kroll, 2010, The geophysical response of the Tupinda Cu-Au-Mo porphyry prospect, Tabar Islands, Papua New Guinea: 21st International Geophysical Conference and Exhibition, ASEG, Extended Abstracts, doi: 10.1071/ASEG2010ab114.
Labson, V., A. Becker, H. Morrison, and U. Conti, 1985, Geophysical exploration with audiofrequency natural magnetic fields: Geophysics, **50**, 656–664, doi: 10.1190/1.1441940.
Legault, J. M., H. Kumar, and B. Milicevic, 2009, ZTEM airborne tipper AFMAG test survey over a magmatic copper-nickel target at Axis lake in Northern Saskatchewan: 79th Annual International Meeting, SEG, Expanded Abstracts, 1272–1276.
Legault, J., and P. Wannamaker, 2014, Two-dimensional joint inversion of ZTEM and MT plane-wave EM data for near surface applications: Presented at the Symposium on the Application of Geophysics to Engineering and Environmental Problems, Expanded Abstracts, 18–23.
Legault, J. M., J. B. Witter, P. Berardelli, S. Lombardo, and M. Orta, 2011, Recent ZTEM airborne AFMAG EM survey results over Reese River and other geothermal test areas: GRC Transactions, **35**, 879–884.
Lo, B., and M. Zang, 2008, Numerical modeling of Z-TEM (airborne AFMAG) responses to guide exploration strategies: 78th Annual International Meeting, SEG, Expanded Abstracts, 1098–1102.
Lowell, J., and J. Guilbert, 1970, Lateral and vertical alteration-mineralization zoning in porphyry copper ore deposits: Economic Geology, **65**, 373–408, doi: 10.2113/gsecongeo.65.4.373.
McClenaghan, L., 2013, Geology and genesis of the newton bulk-tonnage gold-silver deposit, central British Columbia: Master's thesis, The University of British Columbia.
McMillan, W., J. Thompson, C. Hart, and S. Johnston, 1995, Regional geological and tectonic setting of porphyry deposits in British Columbia and Yukon Territory: Porphyry deposits of the northwestern Cordillera of North America: Canadian Institute of Mining, Metallurgy and Petroleum.
Mitchinson, D., R. Enkin, and C. Hart, 2013, Linking porphyry deposit geology to geophysics via physical properties: Adding value to Geoscience BC geophysical data: Geoscience BC, Technical report 2013-14.
Monger, J., and R. Price, 2002, The Canadian Cordillera: Geology and tectonic evolution: CSEG Recorder, **27**, 14–36.
Nelson, J., and M. Colpron, 2007, Tectonics and metallogeny of the British Columbia, Yukon and Alaskan Cordillera, 1.8 Ga to the present: Mineral Deposits of Canada: A synthesis of major deposit-types, district metallogeny, the evolution of geological provinces, and exploration methods: Geological Association of Canada, Mineral Deposits Division.
Nelson, P., and G. Vanvoorhis, 1983, Estimation of sulfide content from induced polarization data: Geophysics, **48**, 62–75, doi: 10.1190/1.1441408.
Oldenburg, D., Y. Li, and R. Ellis, 1997, Inversion of geophysical data over a copper gold porphyry deposit: A case history for Mt. Milligan: Geophysics, **62**, 1419–1431, doi: 10.1190/1.1444246.
Pressacco, R., 2012, Technical report on the initial resource estimate for the Newton project, central British Columbia, Canada: Technical report NI43-101.
Rippe, D., M. Unsworth, and C. Currie, 2013, Magnetotelluric constraints on the fluid content in the upper mantle beneath the Southern Canadian Cordillera: Implications for rheology: Journal of Geophysical Research: Solid Earth, **118**, 5601–5624, doi: 10.1002/jgrb.50255.
Sasaki, Y., M.-J. Yi, and J. Choi, 2014, 2D and 3D separate and joint inversion of airborne ZTEM and ground AMT data: Synthetic model studies: Journal of Applied Geophysics, **104**, 149–155, doi: 10.1016/j.jappgeo.2014.02.017.
Sillitoe, R. H., 2010, Porphyry copper systems: Economic Geology, **105**, 3–41, doi: 10.2113/gsecongeo.105.1.3.
Siripunvaraporn, W., and G. Egbert, 2009, WSINV3DMT: Vertical magnetic field transfer function inversion and parallel implementation: Physics of the Earth and Planetary Interiors, **173**, 317–329, doi: 10.1016/j.pepi.2009.01.013.
Spies, B. R., 1989, Depth of investigation in electromagnetic sounding methods: Geophysics, **54**, 872–888, doi: 10.1190/1.1442716.
Spratt, J., J. Welford, C. Farquharson, and J. Craven, 2012, Modelling and investigation of airborne electromagnetic data, and reprocessing of vibroseis data, from Nechako basin, B.C., guided by magnetotelluric results: Geoscience BC, Report 2012-14.
Thompson, J., 1995, Exploration and research related to porphyry deposits: Porphyry deposits of the northwestern Cordillera of North America: Canadian Institute of Mining, Metallurgy and Petroleum.
Vallee, M. A., R. S. Smith, and P. Keating, 2011, Metalliferous mining geophysics — State of the art after a decade in the new millennium: Geophysics, **76**, no. 4, W31–W50, doi: 10.1190/1.3587224.
Vozoff, K., 1991, The magnetotelluric methods: *in* M. N. Nabighian, ed., Electromagnetic methods in applied geophysics: Volume 2, Application, Investigations in Geophysics 3, 641–712.
Ward, S., 1959, AFMAG — Airborne and ground: Geophysics, **24**, 761–787, doi: 10.1190/1.1438657.
Yang, D., and D. W. Oldenburg, 2012, Three-dimensional inversion of airborne time-domain electromagnetic data with applications to a porphyry deposit: Geophysics, **77**, no. 2, B23–B34, doi: 10.1190/geo2011-0194.1.